

Investigating and Optimizing Insulin Partitioning with Conjugated Au Nanoparticles in Aqueous Two-Phase Systems Using Response Surface Methodology

Ghazal Saki Norouzi and Farshad Rahimpour*

Cite This: *ACS Omega* 2024, 9, 9676–9685

Read Online

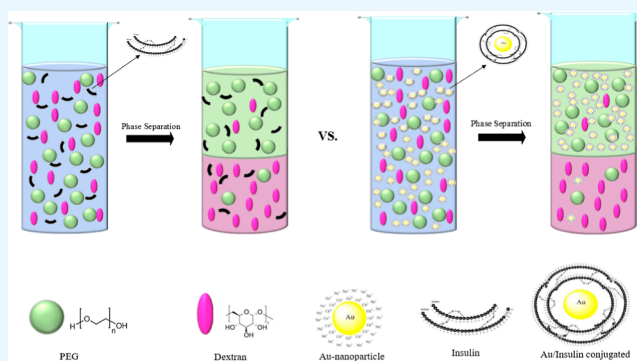
ACCESS |

Metrics & More

Article Recommendations

Supporting Information

ABSTRACT: This study investigated the impact of bioconjugation on the partitioning of insulin, a clinically valuable protein, in an aqueous two-phase system. Gold nanoparticles of different sizes were synthesized and conjugated with insulin. Analysis of the conjugated insulin showed that the insulin remains fully active. Conjugated gold nanoparticles (AuNPs/insulin) were used in polyethylene glycol (PEG)–dextran aqueous two-phase systems to investigate the effect of pH, PEG and dextran molecular weights, PEG and dextran concentrations, AuNPs/insulin dosage, and nanoparticle size on the partition coefficient. These systems were chosen for their biocompatibility and low toxicity. Response surface methodology with D-optimal design was used to model and optimize these systems and their affected parameters. At the optimum condition of a pH = 8 system containing 21% PEG 4000, 5% dextran 100,000, and 100 IU AuNPs/insulin, the partition coefficient of AuNPs/insulin was found to be 192.96, which is in agreement with the empirical partition coefficient of 189.2. This is significantly higher than the partition coefficient of free insulin in a similar system. This approach could be used to overcome limitations in the feasibility of aqueous two-phase systems for industrial-scale purification of biomolecules and biopharmaceuticals.



1. INTRODUCTION

Proteins play a significant role in living systems. Therefore, their isolation, purification, and characterization are of great importance. Over time, purification methods have been upgraded and refined through the development of innovative materials for the enrichment and purification of complex biomolecules.¹ There is significant potential in using an aqueous two-phase system (ATPS) for the extraction, recovery, and purification of a wide range of biological compounds. Compared to other separation methods, ATPS has the advantages of scalability, process integration, biocompatibility, and, most importantly, continuous operation.^{2,3} ATPS consists of two highly aqueous phases, which are typically prepared by dissolving immiscible polymers or a polymer with one or two salts in an aqueous solution.⁴ The immiscibility of the two phases allows favorable partitioning between them to separate and purify different biomolecules.⁵ There is a direct correlation between the partitioning of biomolecules, which is quantified by the partition coefficient (K), and their physicochemical properties. These properties include isoelectric points, sizes, surface hydrophobicity, polymer molecular weight, polymer/salt concentrations, pH, and temperature.^{2,6,7} The separations' selectivity in ATPS has been enhanced under various conditions, which are problematically associated with the need to make structural changes in

ATPSs or to modify biomolecules.^{2,8} It is therefore becoming more necessary to find techniques that do not require the reformulation of system structures or biomolecules. By creating a mechanism that facilitates the transfer of the biomolecule between the two phases, biomolecules partitioning enhances in ATPS.^{9,10} Nanoparticles fulfill this demand and improve biomolecule partitioning. The high surface-to-volume ratio of nanoparticles makes them attractive carriers, which can greatly enhance extraction performance.^{11,12} Inorganic nanoparticles, whose structures exhibit significantly different physical, chemical, and biological properties and functionalities compared to their bulk counterparts, have attracted increasing interest. Especially, concerning noble metal nanoparticles, it has been found that their properties are strongly influenced by their shape and size. Nanoparticle–biomolecule conjugation preserves biomolecule activity and has been widely used in bioanalytical applications.¹³ In particular, nanoparticle–protein conjugates are useful in the emerging field of nanobiotechnol-

Received: December 6, 2023

Revised: January 21, 2024

Accepted: February 8, 2024

Published: February 16, 2024



ogy, such as nanomedicine, drug delivery, and biosensors. This is because the size of nanoparticles is comparable to that of living cells, allowing them to access and act inside the cell. The interaction of the two components has been shown to affect protein surface properties and colloidal stability.^{14–17}

Mohsen Dehnavi et al.¹³ reported a 7-fold increase in enzyme partitioning when using silica-enzyme nanoconjugate carriers in ATPS of polyethylene glycol (PEG) and MgSO_4 compared to nonconjugated systems. Afzal Shoushtari et al.⁹ investigated the ability of Al_2O_3 , TiO_2 , graphene, and graphene oxide (GO) nanoparticles to extract cephalixin in ATPSs containing PEG and three sodium-based organic salts. They found that the partition coefficient for the optimum (PEG + sodium citrate + water) system increased by 59% with the addition of 0.01 wt % GO, while other nanoparticles either had no effect or decreased the partition coefficient. They also concluded that the concentration of nanoparticles can alter the partition coefficient. Nouri et al.¹⁴ developed an organic nanoparticle-based ATPS suitable for a desirable vanillin separation process and revealed the mechanism of partitioning. They showed that the modified system enhanced the partition coefficient of vanillin by 127%. Rahbari et al.¹⁰ conducted a study to evaluate a group of nanoparticles for their ability to partition nisin in ATPS containing PEG and phosphate-based salt. The study showed that the presence of nanoparticles increased the partition factor of nisin 8-fold compared to the ATPS with no nanoparticles.

Among inorganic nanoparticles, gold nanoparticles (AuNPs) have proven to be ideal carriers for bioconjugation applications, as they possess exclusive surface properties, optical properties, stability, and consistency. They also have many advantages, such as ease of synthesis, shape control, and functionalization, which have attracted a wide range of research and biomedical applications.^{18,19} Long and Keating²⁰ conjugated *horseradish peroxidase* to colloidal AuNPs by direct adsorption. They reported for the first time that conjugating protein with AuNPs resulted in remarkable partitioning of biomolecules in ATPS relative to free protein. This concept was employed in some research to achieve better partitioning and purification, as well as to discover promising nanoparticles.²¹

Various factors in ATPSs affect the partition and purification of biomolecules. The governing mechanism of the process variables' effects on the partitioning of biomolecules in ATPS is very complex. These systems are even more complex because the factors involved are not entirely independent of each other. Due to this complexity, it is difficult, and even impossible in some cases, to investigate these effects by complex theoretical thermodynamic models.⁵ One option for investigating the effect of changing parameters and process optimization is to perform experimental tests. Conventional empirical methods are often time-consuming and expensive and may not accurately describe system behavior. Experimental design methods can overcome the limitations of traditional optimization methods. Response surface methodology (RSM) is an experimental design method that models and analyzes complex processes, resulting in the construction of a model that includes efficient independent variables and their interactions under optimal conditions.²²

In this study, polymer–polymer ATPS was selected based on PEG due to its low cost and biocompatibility. To enhance the sustainability of the extraction process and help mitigate environmental issues related to salts and solvent usage and

disposal, more sustainable polymer ingredients, i.e., dextran, are used. Dextran is a biocompatible and biodegradable natural branched polymer consisting of glucose units connected with α -1,6 glycosidic linkages, which is a greener alternative to synthetic polymers and salts.²³ PEG and dextran are widely used together to form ATPS. Both polymers are considered safe for use in biotechnology.^{12,20} This study aimed to investigate the impact of AuNPs on protein partitioning. To achieve this, insulin was conjugated with AuNPs, and its partitioning was examined in PEG–dextran ATPS. The human insulin hormone plays a significant role in regulating carbohydrate metabolism and blood glucose levels. It also affects the metabolism of proteins and lipids.²⁴ Insulin is a protein hormone and cannot be given orally. The only known way to take exogenous insulin is by intramuscular injection. Regular insulin injections are a painful experience for patients. Therefore, an alternative route of insulin delivery is needed. To provide the physiological effect of insulin, it is believed that insulin can be delivered in conjugation with AuNPs. These biological importance of human insulin and its unique characteristics have led to its selection.

To enhance the partitioning of AuNPs/insulin conjugate performance, with the minimum number of required experiments, the operating parameters, including pH, PEG and dextran molecular weights and concentrations, insulin loading amount, and nanoparticle size, and their interactions that affect AuNPs/insulin partitioning were studied and optimized using RSM with a D-optimal design. This technique optimizes complicated systems by evaluating multiple parameters, either alone or in combination with response variables.^{22,25–28}

2. EXPERIMENTAL SECTION

2.1. Materials. Human insulin was supplied by Exir Pharmaceutical Company (Borujerd, Iran). Dextran with average molecular weights of 6000 and 100,000 Da, sodium citrate dihydrate, hydrochloric acid, sodium hydroxide, potassium dihydrogen phosphate, and dipotassium hydrogen phosphate were supplied by Sigma-Aldrich (München, Germany). PEG with average weights of 1000, 4000, and 6000 Da and hydrogen tetrachloroaurate ($\text{HAuCl}_4 \cdot 3\text{H}_2\text{O}$) were attained from Merck (Darmstadt, Germany). All materials were of analytical grade and used as received. Double distilled water was used in all experiments.

2.2. Instrumentation and Equipment. The partitioning of bulk insulin and AuNPs/insulin conjugate was determined using a Unico-S2100 UV diode-array UV/visible spectrometer. The AuNPs/insulin conjugates were separated using a Tuttingen-D78532 centrifuge. Transmission electron microscopy (TEM) images of nanoparticles were captured using a Philips-EM208 instrument. Dynamic light scattering (DLS) images of nanoparticles and AuNPs/insulin conjugates were recorded using a Zetasizer (ZEN3600, Malvern Instruments, UK). The Bomem-MB 104 was used to obtain the Fourier transform infrared (FTIR) spectroscopy. The concentration of PEG and dextran in ATPS was measured with a refractometer (EUROMEX-RD365) and a polarimeter (WZZ-2A).

2.3. Insulin/Gold Nanoparticle Conjugation. AuNPs with diameters 10, 20, and 30 nm were synthesized according to Grabar et al.²⁹ with some modifications. Briefly, to synthesize 10 nm nanoparticles, a solution of 125 mL $\text{HAuCl}_4 \cdot 3\text{H}_2\text{O}$ (0.254 mM) was added to a 250 mL round-bottom flask and heated to boiling temperature while being vigorously stirred by a magnet. To maintain the solution

volume, a balloon was connected to the refrigerant. After boiling, 12.5 mL of a 40 mM sodium citrate solution was immediately added to the gold solution. Within a few minutes, the solution color was changed from yellow to red, indicating the formation of AuNPs. The solution was boiled for 10 min and stirred for 15 min. The balloon was then cooled in a water bath until it reached room temperature. To prepare 20 nm nanoparticles, 0.01 g of $\text{HAuCl}_4 \cdot 3\text{H}_2\text{O}$ was dissolved in 100 mL of distilled water to create a 0.01% (w/v) gold solution. Next, a 1% (w/v) solution of sodium citrate was added. The solutions were then equilibrated in a hot water bath at 60 °C for approximately 20 min. The gold solution obtained was transferred to a flask connected to a refrigerant. Then, 2 mL of sodium citrate solution was added to the mixture, stirred vigorously, and heated until boiling. After 15 min, the solution turned dark red. The solution was boiled for an additional 5 min after the color change was observed. The heat was then turned off, and the reaction mixture was stirred for another 15 min. Finally, the flask was placed in a cold water bath to cool down to room temperature. To synthesize 30 nm nanoparticles, 30 mL of 20 nm AuNPs from the previous step were added to 100 mL of $\text{HAuCl}_4 \cdot 3\text{H}_2\text{O}$ solution with a concentration of 0.01% (w/v). The resulting mixture was transferred to a balloon connected to a refrigerant and heated to boiling temperature. Next, 1 mL of 1% (w/v) sodium citrate solution was added to the flask. The mixture was stirred vigorously and boiled for 15 min. The heat was then turned off, and the mixture was allowed to cool slowly to room temperature.

A 0.07 mM insulin solution was prepared by adding a calculated amount of insulin to colloidal Au solutions. The suspension was incubated for 24 h at 15 °C and then centrifuged at 30,000g for 30 min. The pellet obtained was separated from the supernatant and redispersed in a 0.01 M HCl solution to remove nonconjugated insulin. [Figure 1](#)

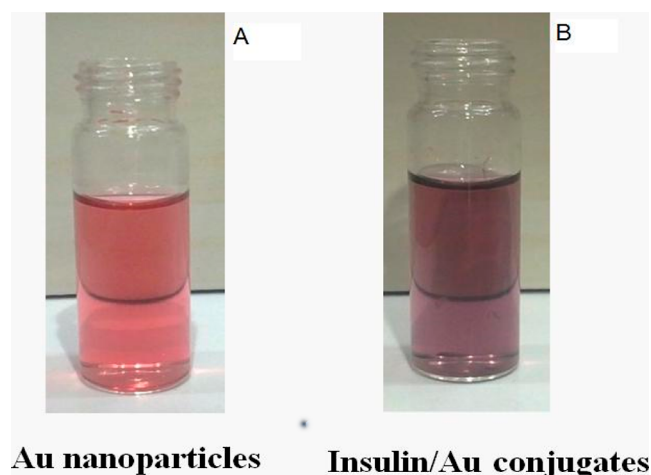


Figure 1. (A) AuNP solution; (B) AuNPs/insulin conjugate solution.

displays the AuNP solution before and after insulin conjugation. Insulin-conjugated AuNPs were identified using UV-vis ([Figure S1](#)), TEM ([Figure S2](#)), DLS ([Figure S3](#)), and FTIR ([Figure S4](#)) techniques, as presented in the [Supporting Information](#).

2.4. Partitioning. To study the effect of AuNPs on insulin partitioning, two types of systems were prepared: (1) insulin systems consisting of dextran, PEG, buffer, and insulin

solution. (2) Insulin/AuNP systems were prepared using dextran, PEG, buffer, and insulin/AuNP solution. The control (blank) systems used in this study consisted of dextran, PEG, and buffer with the same composition as the examined systems. These control systems were employed to eliminate the effects of component interference.

The stock insulin solution was prepared by dissolving a specific amount of insulin powder in a small amount of 0.01 M HCl until the powder dissolved. The final volume was adjusted to 50 mL by adding NaOH + NaH_2PO_4 buffer, pH 7.4.

PEG, dextran, and aqueous buffer solution were introduced into test tubes in appropriate quantities and agitated vigorously. The final weight of 4 g was achieved by adding either AuNPs/insulin solution or insulin solution. The mixtures were stirred gently to prevent foaming. After incubation for 24 h at 25 °C, the tubes were centrifuged at 3000g for a few minutes to clarify the interface. After the separation of the two phases, the insulin concentration was determined for each phase using a UV/visible spectrometer. If the phases were too viscous, they were diluted to allow for insulin analysis. The partition coefficient, K , was calculated as the insulin concentration at the top phase divided by the insulin concentration at the bottom phase.

2.5. Experimental Design. The RSM is a significant branch of experimental design. It combines statistical and mathematical approaches to improve, develop, and optimize processes.²² To enhance the precision of the estimated model, the D-optimal design is commonly used to create second-order response surface models with quantitative factors. A D-optimal design is often selected because the concept of minimizing regression coefficient variance is intuitively appealing.³⁰ It allows for fewer experimental runs compared to any classical design available. The D-optimal design is a useful alternative when classical symmetrical designs are not applicable. This can happen when the number of experiments chosen by a classical design is too large, if the experimental region has an irregular shape, or if other than the usual first or second-order models are desired.²²

MODDE 8.0 from Umetrics (Umea, Sweden) was used to determine the most appropriate conditions for partitioning AuNPs/insulin utilizing a D-optimal design for the second-order response surface model. The selection of levels for independent variables was based on the primary experiments run before designing the experiments. [Table 1](#) shows the experimental range and levels of independent variables determined from preliminary studies. The experimental design consisted of a matrix comprising center points, vertical axis

Table 1. Factors and Levels in the Seven-Factor D-Optimal Response Surface Design to Optimize AuNPs/Insulin Partitioning

independent variables	factor	level		
		low	center	high
pH	X_1	5	7	9
PEG molecular weight	X_2	1000	4000	6000
dextran molecular weight	X_3	6000		100,000
PEG concentration (wt %)	X_4	17	19	21
dextran concentration (wt %)	X_5	5	7	9
nanoparticle size (nm)	X_6	10	20	30
insulin solution load (I.S.L) (IU/mL)	X_7	50		100

Table 2. Experimental Design for the Partitioning Coefficients of Insulin and AuNPs/Insulin in PEG–Dextran ATPSs

run	X ₁	X ₂	X ₃	X ₄	X ₅	X ₆	X ₇	K _{AuNPs/insulin}	K _{insulin}
1	5	1000	6,000	17	9	10	50	4.02 ± 0.12	0.32 ± 0.07
2	5	1000	6,000	21	5	10	50	4.61 ± 0.14	0.41 ± 0.09
3	9	1000	6,000	21	9	10	50	24.60 ± 0.74	4.87 ± 0.12
4	9	1000	100,000	17	5	10	50	82.95 ± 0.41	12.88 ± 0.28
5	5	1000	100,000	21	9	10	50	7.87 ± 0.09	0.82 ± 0.11
6	5	6000	6,000	17	5	10	50	2.34 ± 0.06	0.19 ± 0.04
7	5	6000	6,000	21	9	10	50	2.95 ± 0.07	0.23 ± 0.05
8	9	6000	100,000	17	9	10	50	69.02 ± 0.69	9.04 ± 0.23
9	9	6000	100,000	21	5	10	50	78.08 ± 0.71	9.31 ± 0.22
10	5	1000	6,000	21	9	10	100	15.64 ± 0.23	0.51 ± 0.06
11	9	1000	100,000	17	9	10	100	90.61 ± 0.66	17.82 ± 0.37
12	9	1000	100,000	21	5	10	100	95.01 ± 0.89	6.87 ± 0.16
13	5	4000	100,000	17	5	10	100	158.01 ± 0.95	20.43 ± 0.48
14	9	6000	6,000	17	5	10	100	32.88 ± 0.59	0.87 ± 0.27
15	9	6000	6,000	21	9	10	100	50.66 ± 0.71	7.23 ± 0.19
16	5	6000	100,000	21	9	10	100	55.60 ± 0.43	0.76 ± 0.08
17	7	4000	6,000	19	7	20	100	8.46 ± 0.08	7.33 ± 0.17
18	5	1000	6,000	21	9	30	50	3.47 ± 0.09	0.26 ± 0.05
19	9	1000	100,000	17	9	30	50	128.78 ± 0.91	13.30 ± 0.32
20	9	1000	100,000	21	5	30	50	141.47 ± 0.95	14.64 ± 0.35
21	9	4000	6,000	17	5	30	50	52.61 ± 0.88	5.78 ± 0.17
22	9	6000	6,000	21	9	30	50	40.21 ± 0.28	4.22 ± 0.10
23	5	6000	100,000	17	5	30	50	15.32 ± 0.09	0.48 ± 0.02
24	5	6000	100,000	21	9	30	50	5.74 ± 0.05	0.54 ± 0.08
25	5	1000	6,000	17	5	30	100	6.90 ± 0.07	0.45 ± 0.11
26	9	1000	6,000	17	9	30	100	60.67 ± 0.37	6.12 ± 0.14
27	9	1000	6,000	21	5	30	100	55.60 ± 0.49	6.90 ± 0.16
28	5	1000	100,000	17	9	30	100	11.83 ± 0.05	1.15 ± 0.09
29	5	1000	100,000	21	5	30	100	19.13 ± 0.08	1.80 ± 0.14
30	9	4000	100,000	21	9	30	100	151.94 ± 0.89	12.65 ± 0.44
31	5	6000	6,000	17	9	30	100	4.68 ± 0.03	0.41 ± 0.13
32	5	6000	6,000	21	5	30	100	5.34 ± 0.07	0.33 ± 0.05
33	9	6000	100,000	17	5	30	100	144.58 ± 0.92	15.20 ± 0.36
34	7	6000	100,000	19	7	30	100	141.05 ± 0.85	13.52 ± 0.31
35	7	6000	100,000	19	7	30	100	138.21 ± 0.97	12.98 ± 0.24
36	7	6000	100,000	19	7	30	100	139.94 ± 0.95	13.64 ± 0.22

points, center edge points, and axial points to obtain a comprehensive response throughout the matrix.

The correlation between the response and the selected variables can be expressed by eq 1²⁵

$$Y = \beta_0 + \sum_{i=1}^n \beta_i x_i + \sum_{i=1}^n \beta_{ii} x_i^2 + \sum_{i<1} \sum_{j=1}^n \beta_{ij} x_i x_j \quad (i < j) \quad (1)$$

where Y , β_0 , β_i , β_{ii} , and β_{ij} are the partitioning factor, the constant coefficient (intercept term), the linear coefficients, the quadratic coefficients, and the interaction coefficients, respectively. The parameters x_i and x_j are independent variables and n is the number of factors.

Significant variables were analyzed using variance analysis (ANOVA). Fisher's satirical test (F -test) was used to evaluate the significance of the proposed model. An F -value represents the significance of each controlled variable in the model when it is determined by comparing the mean square of regression ($MS_{\text{regression}}$) with the residual (MS_{residual}).³¹ The data obtained for each parameter with the experimental design was fitted to the second-order model using multiple regression. Interactions between the independent variables result in the predicted response. The most appropriate model was selected as the one

with the highest coefficient of multiple determination (R^2), the most significant model p -value (probability of error), and reasonable agreement between the predicted R^2 and the adjusted R^2 . A nonsignificant lack of fit p -values should also be considered.³²

3. RESULTS

3.1. Partitioning and Model Analysis. When separating a compound from a mixture, there are interactions between the components of the mixture, as well as between the compound and the phases. Most studies in this field are empirical, and purification is evaluated by manipulating certain factors. The traditional approach to optimizing production by changing one factor at a time is very time-consuming and does not reveal the interactive effects of independent variables. The design matrix of the variables and partition coefficients of insulin and AuNPs/insulin in PEG and dextran ATPSs are presented in Table 2. A total of 36 experiments were conducted, including 3 center points, 28 model points (vertical axis points, center edge points, and axial points), and 5 additional experiments to estimate the lack of fit in the model. Each experiment was run in triplicate, and the average of the data obtained was used as the response for each experiment. Standard deviations were

calculated in each case to confirm the reproducibility of the experimental data.

The partition coefficients of insulin and AuNPs/insulin indicate that conjugation with AuNPs enhances insulin separation in all systems. This is caused by an increase in the surface area due to insulin surface absorption on the nanoparticle surface and an increase in the surface charge of AuNPs. As a result, insulin is highly partitioned in the upper phase (PEG-rich phase).

Regression analysis was conducted to examine how the variation in the process independent variables is related to the variation in the partitioning. The coefficients in the regression indicate the magnitude of these changes, while the p -values indicate whether these coefficients are significantly different from zero. All the direct relationships between independent variables and response are considered as main effects. However, sometimes the influence of another variable changes this relationship between an independent variable and response; this is called the interaction effect. If statistically significant interaction effects exist, the main effects cannot be interpreted without considering the interactions. In a multi-variable model, all main effects and their interactions should be included in the first step of the fit. Variables that do not provide a contribution to the model should be eliminated, and a new, smaller model should be fitted. The original and reduced models should then be compared using an F -test to ensure that the reduced model fits as well as the original model. If the change in coefficients exceeds 20%, it is important to consider the impact of the deleted variables on the remaining variables. In such cases, it is recommended to add the deleted variables back to the model. A model is modified by removing and adding variables and refitting it until all of the removed variables are statistically insignificant and those remaining in the model are significant. This simplifies the model and increases the precision of predictions. The criterion for model reduction is the statistical significance of a term. Eliminating statistically insignificant terms can improve the precision of predictions from the model. The statistical significance criterion aims to find a model that meets our goals, but it does not always yield the best model. Other statistical criteria, such as adjusted R^2 and predicted R^2 (or Q^2), can also be used to reduce a model. Best subsets regression uses R^2 to identify the best models, which may or may not include only statistically significant terms.^{5,22}

The result of the above model reduction was a modified quadratic model. This model was used to describe the effects of the studied variables and their interaction, as shown in eq 2

$$Y = 144.694 + 35.4413X_1 + 14.7942X_3 - 57.1377X_1^2 - 35.8359X_2^2 + 20.1276X_1X_3 + 8.94902X_3X_6 - 8.19322X_6X_7 \quad (2)$$

Table 3 presents the regression coefficients and their corresponding p -values, which were used to identify significant parameters. The R^2 and adjusted R^2 were 0.911 and 0.864, respectively. R^2 measures the reduction in Y variability achieved by using the regression variables in the model and ranges from zero to one. A higher R^2 indicates a stronger model with better predictive capabilities. The R^2 value represents the variation in the response due to independent variables and their interaction. This value indicates that the model can explain 91.1% of the variability in the response.

Table 3. Model Regression Coefficients and Their Probability of Error (p -Value) in the Second-Order AuNPs/Insulin Partitioning Model

real variables	coded variable	coefficient	p -value
constant	constant	144.694	3.26×10^{-11}
pH	X_1	35.4413	1.06×10^{-9}
PEG MW	X_2	0.685803	0.862805
dextran MW	X_3	14.7942	0.000364
PEG %	X_4	4.17472	0.237653
dextran %	X_5	-1.55903	0.65495
nanoparticle size	X_6	2.71168	0.441232
insulin solution load (I.S.L)	X_7	7.26306	0.051573
pH \times pH	$X_1 \times X_1$	-57.1377	0.002182
PEG MW \times PEG MW	$X_2 \times X_2$	-35.8359	0.004161
pH \times dextran MW	$X_1 \times X_3$	20.1276	9.72×10^{-6}
dextran MW \times nanoparticle size	$X_3 \times X_6$	8.94902	0.015989
I.S.L \times nanoparticle size	$X_7 \times X_6$	-8.19322	0.030474

R^2_{adjust} can be used to determine the reduction in response variability by regression variables in the model. In fact, the addition of unnecessary terms often decreases the value of R^2_{adjust} .²² In this case, R^2 and R^2_{adjust} are close to each other, suggesting that all the terms used are necessary for constructing the appropriate model. The Q^2 (cross-validation) was 0.705, indicating the predictive value of endogenous constructs.

Table 4 presents the ANOVA results for the model. The model's adequacy of fit is represented by the F -value of 196

Table 4. Analysis of Variance Results for the Modified Second-Order Model of AuNPs/Insulin Conjugate Partitioning Coefficient in ATPS^a

partitioning coefficient	DF	SS	MS	F	P
total	36	215,412	5983.68		
regression	12	90,998.2	7583.18	196.00	0.000
residual	23	8,898.64	38.689		
lack of fit	20	6,084	304.2	0.949	0.324
pure error	3	2,814	938.216		

^aDF: degree of freedom, SS: sum of squares, MS: mean of squares, F : F -factor, P : probability of error, $R^2 = 0.911$, $R^2_{\text{adj}} = 0.864$, $Q^2 = 0.705$.

and corresponding p -value of 0.000, which means that the model was accurate. Additionally, the model lack of fit error probability is evidenced by a high p -value of 0.324, indicating that it accurately represents the relationships between parameters within the selection range.²⁵ Figure 2 shows that the predicted and experimental partitioning efficiency values were reasonably comparable, providing evidence for the validity of the regression model. Table 3 illustrates the significance of main effects and their interactions on AuNPs/insulin partitioning. The main effects of pH (X_1) and dextran molecular weight (X_3), interactive terms ($X_1 \times X_3$, $X_3 \times X_6$, and $X_6 \times X_7$), and quadratic model terms (X_1^2 , X_2^2) significantly affected AuNPs/insulin partitioning. Increasing the pH (X_1) and dextran MW (X_3) have positive effects on partitioning coefficients. The quadratic signs of pH (X_1^2) and PEG MW (X_2^2) are negative, indicating that there is a maximum with respect to these variables. The positive interaction effects of $X_1 \times X_3$ and $X_3 \times X_6$ mean that increasing dextran molecular

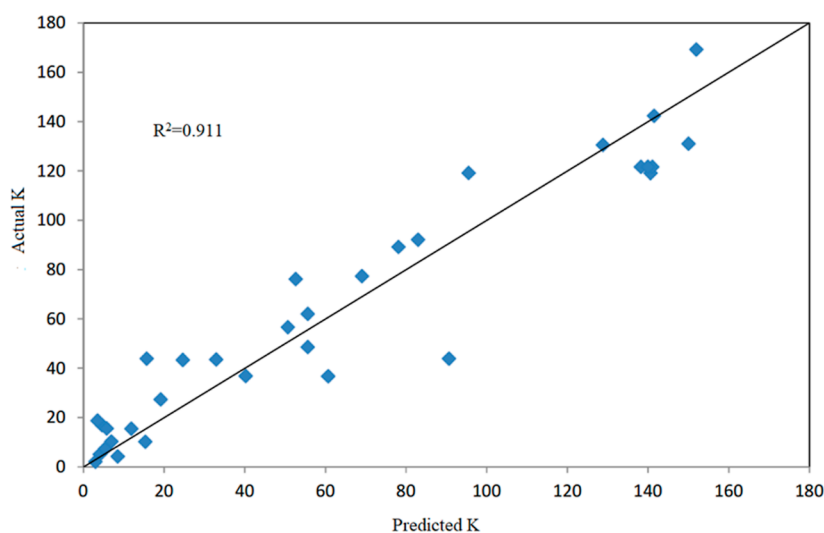


Figure 2. Comparison of actual and predicted partitioning coefficient (K) of AuNPs/insulin.

weight while simultaneously increasing pH and nanoparticle size results in an increase in the partition coefficient. The negative interaction effect of $X_6 \times X_7$ means that the partitioning coefficient decreases with a simultaneous rise in nanoparticle size and AuNPs/insulin load.

3.2. Model Validation. The partitioning coefficient of the AuNPs/insulin conjugate in PEG–dextran systems was optimized using MODDE software. The highest partitioning coefficient value was achieved for a system with a pH of 8, 21% PEG 4000, 5% dextran 100,000, AuNPs/insulin 100 (IU/mL), and 30 nm AuNPs, resulting in a partition coefficient of 192.96. An experiment was conducted using the predicted system to confirm the model's predicted results. The actual partition coefficient was found to be 189.2. The experimental value closely matches the expected value, indicating successful validation of the model.

4. DISCUSSION

Various analytical tools have been used to determine the efficiency of protein binding to AuNPs. These methods have been employed to fully characterize bioconjugated nanoparticle systems and provide varying levels of quantitative information about the physicochemical state of a given system. The most effective methods are UV/vis extinction spectra, DLS, TEM, and FTIR.³³ UV–vis spectrum was measured for conformation of the AuNP formation and insulin-conjugated AuNPs. The UV–vis spectra of the AuNP solution before and after insulin conjugation are shown in Figures S1.1 to S1.3. The spectrum indicates that the surface plasmon resonance peak (λ_{SPR}) increases as the nanoparticle size increases. λ_{SPR} are 519, 522, and 525 nm for the sizes of 10, 20, and 30 nm, respectively. This adsorption could be attributed to the surface plasmon vibrations excited in the AuNPs. The addition of insulin to the nanoparticle solutions causes a shift to higher wavelengths in the λ_{SPR} of the nanoparticles, indicating the absorption of insulin molecules on the surface of AuNPs. When insulin is conjugated to AuNPs, the λ_{SPR} increases to 531, 532, and 538 nm for 10, 20, and 30 nm nanoparticles, respectively. The absorption peak related to insulin at $\lambda_{\text{SPR}} = 275$ nm is visible after it is placed on AuNPs, as shown in Figures S1.1 to S1.3. TEM images of AuNPs and insulin-conjugated nanoparticles (Figure S2) showed that the overall

arrangement of nanoparticles was unaffected, and thus the observed band shift after insulin coverage was due to conjugation of insulin and not nanoparticle aggregation. One useful method of protein detection used in bioconjugation systems is the DLS assay. This assay is a simple, one-step, rapid, sensitive, and accurate method. When the proteins are introduced to the AuNPs, they bind around them and form larger aggregates. DLS measurement confirmed the size variation of the nanoparticles (Figure S3). For example, in 30 nm nanoparticles before the addition of insulin, a uniform, narrow peak at 30 nm is observed (Figure S3.1). After the formation of AuNPs/insulin conjugates, their size increases, resulting in a shift of the peak to a higher value (at 220 nm), as observed in the DLS histogram (Figure S1.2). The DLS data on nanoparticle size is also confirmed by the TEM image (Figure 2S), which shows the formation of almost uniform-size nanoparticles.

Figure S.4 shows the FTIR spectra of AuNPs before insulin conjugation, pure insulin, and AuNPs after insulin conjugation. The peaks at 1078 cm^{-1} (C–O stretching), 1394 cm^{-1} (symmetric C=O stretching), 1583 cm^{-1} (asymmetric C=O stretching), and $2850\text{--}3700\text{ cm}^{-1}$ (O–H stretching) observed in the AuNP spectrum show the presence of citrate around the AuNPs. In single-phase AuNP synthesis methods, sodium citrate has both stabilizing and reducing roles, and by forming a layer around the nanoparticles, it prevents them from aggregating.¹⁹ By comparing these spectra, it can be concluded that by introducing insulin to the solution of AuNPs, citrate ions have been replaced by insulin molecules. The peaks associated with citrate disappear, and new peaks similar to those of pure insulin spectra are observed. These peaks appear at 1223 cm^{-1} (C–N stretching), 1442 and 1543 cm^{-1} (amid II C–H bending), 1631 cm^{-1} (amide I vibrational mode, which can be assigned to random secondary structures visible in the active insulin sample), 2960 cm^{-1} (CH_3), 3074 cm^{-1} (sp^2 for C=C–H), 3286 cm^{-1} (amide N–H stretching), and 3431 cm^{-1} (C–H stretching).³⁴ These peaks confirm the presence of insulin on the surface of the nanoparticles. In addition, the comparison of the spectra for insulin and AuNPs/insulin conjugate does not show any significant changes in the secondary structure of insulin, confirming that the interaction

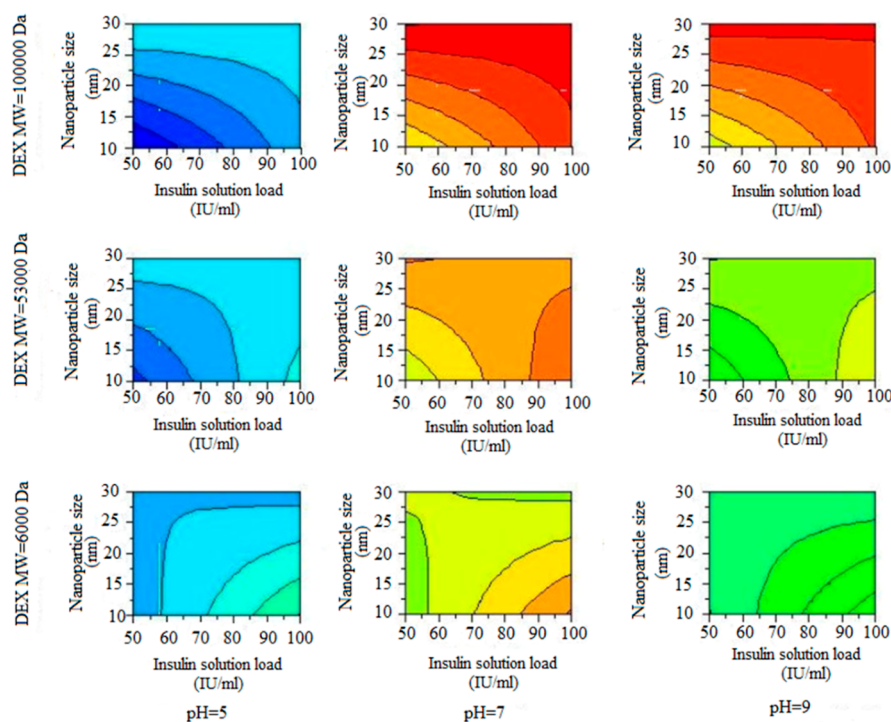


Figure 3. AuNPs/insulin partition coefficient constant response contours at 21% PEG 4000 and 5% dextran as a function of nanoparticle size and dosage of AuNPs/insulin load for different pH and dextran molecular weights.

of insulin with the AuNPs does not affect the structural stability of insulin.³⁵

Figure 3 shows the constant response contours of AuNPs/insulin partitioning coefficient based on pH, dextran MW, nanoparticle size, and AuNPs/insulin load at 21% PEG 4000 and 5% dextran. The partition coefficient increases as the color changes from blue to red. The partitioning coefficient also increases with increasing dosage of AuNPs/insulin and nanoparticle size, as well as with rising pH and dextran MW.

To better understand the effect of operating variables on partitioning, 3D graphs were plotted for the response variable against two independent variables while keeping the other five variables constant. Figures 4–6 present these plots. The optimal condition is indicated by red color in the 3D plots. Figure 4 shows how the partitioning coefficient is affected by the interaction between pH and dextran MW. The coefficient increases as the molecular weight of dextran increases, reaching a maximum at pH 8 and then decreases as pH increases to 9.

To comprehend the correlation between the partition coefficient of a biomolecule and the pH of the system, it is necessary to consider the nature of the charged amino acid residues on the surface of the biomolecule and electrostatic interactions between the biomolecule and polymers.^{2,36} The partitioning results (shown in Table 2) indicate that at pH 5, insulin partitioned into the dextran-rich phase, whereas AuNPs/insulin partitioned into the PEG-rich phase. However, at a pH above 7, the partitioning of insulin and AuNPs/insulin occurred in the PEG-rich phase. At a pH of 5, the conjugation to AuNPs changed the phase preference of insulin, whereas at the other two pH values tested, the conjugation improved the phase preference of insulin. Generally, negatively charged biomolecules prefer the upper phase (PEG-rich phase), while positively charged biomolecules partition to the lower phase (dextran-rich phase). When the pH of a biomolecule rises above its isoelectric point (pI), it becomes more negative,

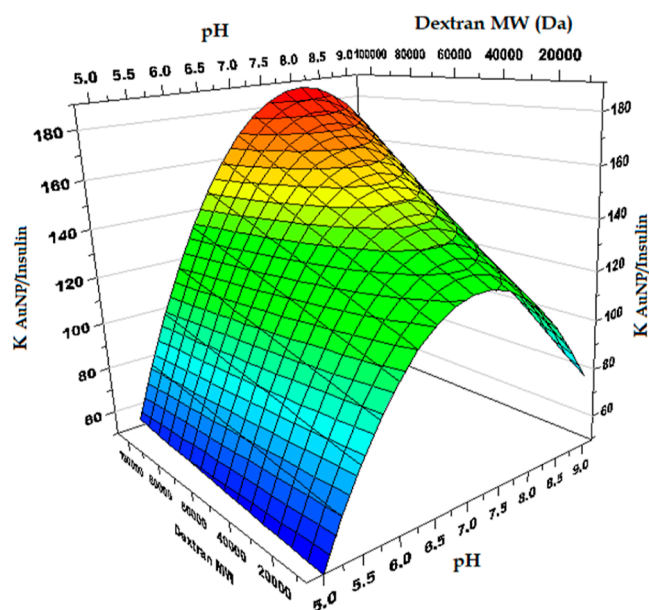


Figure 4. 3D response surface graph for partitioning coefficient of AuNPs/insulin as a function of pH and dextran molecular weight [the other variables were kept constant at 21% PEG 4000, 5% dextran, AuNPs/insulin 100 (IU/mL), and 30 nm AuNPs].

resulting in an increase in the partition coefficient.^{2,37} Changes in pH causes a shift in the phase preference due to variations in insulin surface charge (pI = 5.4), and the magnitude of partitioning depends on surface charges. The decrease in the partitioning coefficient between pH 8 and 9 may be attributed to changes in the insulin molecular structure and its interaction with the aqueous environment, e.g., hydrophobic interactions.^{38,39} The conjugation to AuNPs changed the surface properties, and the high surface charge of the AuNPs

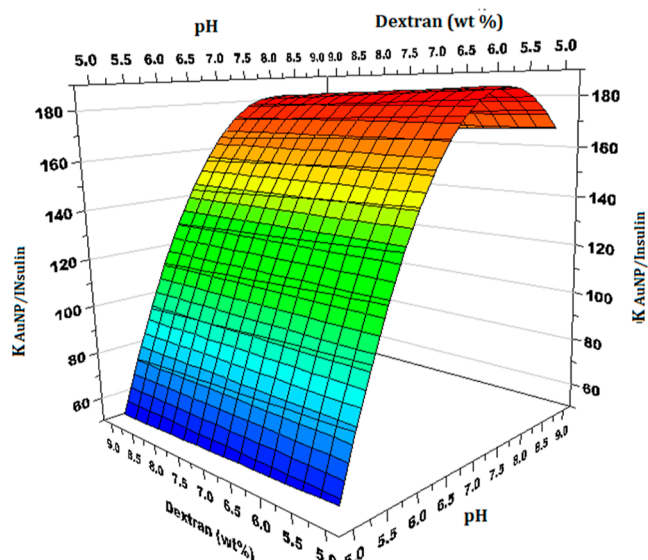


Figure 5. 3D response surface graph for partitioning factors as a function of pH and concentration of dextran [the other variables were kept constant at 21% PEG 4000, dextran 100,000, AuNPs/insulin 100 (IU/mL), and 30 nm AuNPs].

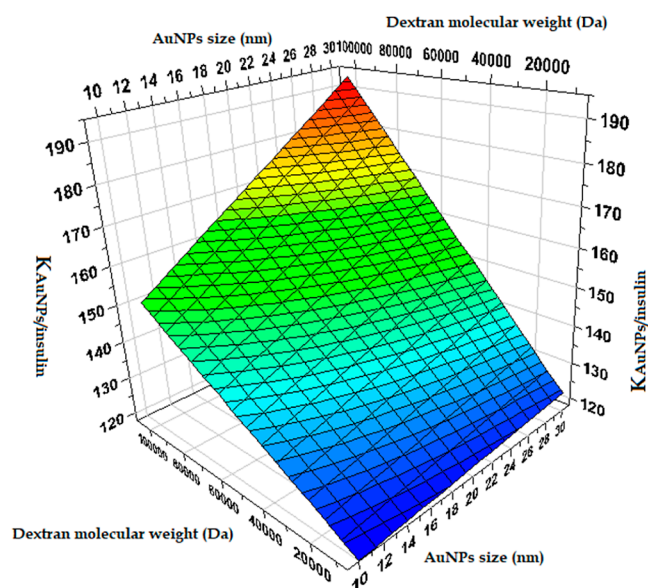


Figure 6. 3D response surface graph for partitioning factors as a function of nanoparticle size and dextran molecular weight [the other variables were kept constant at pH 8, 21% PEG 4000, 5% dextran, and AuNPs/insulin 100 (IU/mL)].

contributes to their excellent partitioning.^{20,40} Also, as the molecular weight of dextran increases, the gap between polymer networks decreases, reducing the space available for molecules in the dextran phase. This leads to the volume exclusion effect, which causes the biomolecules to partition into the PEG phase, resulting in an increase in the AuNPs/insulin partition coefficient.⁴¹ Figure 5 shows the impact of pH changes on the partitioning factor, whereas dextran concentration has no effect in the selected range.

Figure 6 illustrates the interactive effect of nanoparticle size and dextran molecular weight. It is evident that at higher dextran molecular weight, an increase in nanoparticle size has a greater impact. Solute size has been reported to be a key factor

in determining the partition coefficient in an ATPS.^{2,42} However, it is challenging to explain the impact of size due to the lack of control over other variables, such as shape, presence, distribution of charged, hydrophobic, and hydrophilic groups on the biomolecule surface.^{43,44} In this study, different sized AuNPs/insulin conjugates were used to investigate the effects of size on partitioning. The model demonstrates a significant correlation between AuNPs/insulin partitioning and conjugate size. An increase in the surface area of AuNPs from 10 to 30 nm enhanced the partition coefficient. The study shows that the size of AuNPs can greatly affect the degree of partitioning and that conjugates may also demonstrate significant partitioning.⁴⁰

According to the model, the optimal molecular weight of PEG is 4000. Increasing the molecular weight from 1000 to 4000 intensifies PEG hydrophobicity, resulting in the strongest interaction with insulin. However, when the molecular weight exceeds 6000, the partition coefficient decreases due to excluded volume effects.

Increasing the amount of AuNPs/insulin to the system can allow more particles to be interspersed between the polymer chains. It is important to note that increasing the AuNPs/insulin dosage to a certain level results in an increase in the partition coefficient. However, if the amount of AuNPs/insulin exceeds a certain value, the interaction between the polymer and insulin decreases due to AuNPs/insulin accumulation in the polymer chain. This leads to a decrease in the partition coefficient.

5. CONCLUSIONS

This study demonstrates the use of AuNP bioconjugation as having excellent potential to enhance protein purification in ATPS. It was observed that the biological stability of insulin is not affected by bioconjugation. The obtained results indicate that the AuNPs/insulin bioconjugate system has a superior extraction efficiency (more than 10 times) compared to the insulin systems. The effect of different operating parameters on the AuNPs/insulin partition behavior was investigated. The partition coefficient of the bioconjugate is significantly affected by pH, dextran MW, and AuNPs/insulin dosage. Furthermore, simultaneous changes in these parameters with nanoparticle size and polymer MW have interactive effects on protein recovery. The optimization of this process is achieved by employing RSM as a potential technique. At the optimum operation conditions: pH of 8, 21% PEG 4000, 5% dextran 100,000, AuNPs/insulin 100 (IU/mL), and 30 nm AuNPs, a partition coefficient of 192.96 was achieved. An extremely good agreement was obtained between the experimental and predicted results, hence verifying the validity of the model. This work can provide a new practical approach for the extraction, recovery, and purification of higher-purity, valuable biological compounds for use in the biopharmaceutical industry.

■ ASSOCIATED CONTENT

Supporting Information

The Supporting Information is available free of charge at <https://pubs.acs.org/doi/10.1021/acsomega.3c09664>.

UV–visible spectroscopy measurements of AuNPs and AuNPs/insulin; TEM measurements of AuNPs and AuNPs/insulin; DLS of AuNPs and AuNPs/insulin; and

FTIR spectra of insulin, AuNPs, and AuNPs/insulin (PDF)

AUTHOR INFORMATION

Corresponding Author

Farshad Rahimpour – Biotechnology Research Laboratory, Chemical Engineering Department, Faculty of Petroleum and Chemical Engineering, Razi University, Kermanshah 67144-14971, Iran; orcid.org/0000-0002-8564-9436; Phone: +98 83 34343345; Email: f_rahimpour@razi.ac.ir, f_rahimpour65@yahoo.com; Fax: +98 83 34343321

Author

Ghazal Saki Norouzi – Biotechnology Research Laboratory, Chemical Engineering Department, Faculty of Petroleum and Chemical Engineering, Razi University, Kermanshah 67144-14971, Iran

Complete contact information is available at:

<https://pubs.acs.org/10.1021/acsomega.3c09664>

Author Contributions

G.S.N.: conducting the experiments, methodology, and writing the original draft of the manuscript. F.R.: supervision, designing the research, methodology, participating in the discussion on the data, and writing-review and editing.

Notes

The authors declare no competing financial interest.

ACKNOWLEDGMENTS

The authors are grateful to the research vice department of Razi University for partially supporting them in the accomplishment of the work.

REFERENCES

- (1) Le, T.-D.; Suttikhana, I.; Ashaolu, T. J. State of the art on the separation and purification of proteins by magnetic nanoparticles. *J. Nanobiotechnol.* **2023**, *21*, 363.
- (2) Singla, M.; Sit, N. Theoretical Aspects and Applications of Aqueous Two-Phase Systems. *ChemBioEng Rev.* **2023**, *10* (1), 65–80.
- (3) Mo, Y. L.; Fischlschweiger, M.; Zeiner, T. Polymeric Aqueous Two Phase System with an Immobilized Phase by Cross-Linking. *Ind. Eng. Chem. Res.* **2022**, *61* (41), 15381–15389.
- (4) Hatti-Kaul, R. Aqueous two-phase systems. In *Aqueous Two-Phase Systems: Methods and Protocols*; Hatti-Kaul, R., Ed.; Humana Totowa: NJ, 2008; Vol. 11, pp 1–10.
- (5) Rahimpour, F.; Hatti-Kaul, R.; Mamo, G. Response surface methodology and artificial neural network modelling of an aqueous two-phase system for purification of a recombinant alkaline active xylanase. *Process Biochem.* **2016**, *51* (3), 452–462.
- (6) Lira, R. B.; Willersinn, J.; Schmidt, B. V. K. J.; Dimova, R. Selective Partitioning of (Biomacro)molecules in the Crowded Environment of Double-Hydrophilic Block Copolymers. *Macromolecules* **2020**, *53* (22), 10179–10188.
- (7) Chen, Y.; Liang, X.; Kontogeorgis, G. M. Optimal Design of Aqueous Two-Phase Systems for Biomolecule Partitioning. *Ind. Eng. Chem. Res.* **2023**, *62* (28), 11165–11177.
- (8) Enriquez-Ochoa, D.; Meléndez-Martínez, D.; Aguilar-Yáñez, J. M.; Licona-Cassani, C.; Mayolo-Deloiisa, K. Development of aqueous two-phase systems-based approaches for the selective recovery of metalloproteases and phospholipases A2 toxins from *Crotalus molossus nigrescens* venom. *Bioresour. Bioprocess.* **2021**, *8*, 136.
- (9) Afzal Shoushtari, B.; Rahbar Shahrouzi, J.; Pazuki, G. Effect of Nanoparticle Additives on Partitioning of Cephalixin in Aqueous Two-Phase Systems Containing Poly(ethylene glycol) and Organic Salts. *J. Chem. Eng. Data* **2016**, *61* (7), 2605–2613.
- (10) Rahbari, N.; Shahriari, S.; Pazuki, G. Separation Process of Nisin Using Aqueous Two-Phase Systems: A New Approach Featuring Nanoparticles. *J. Chem. Eng. Data* **2020**, *65* (4), 2212–2219.
- (11) Dharmesh, E.; Stealey, S.; Salazar, M. A.; Elbert, D.; Zustiak, S. P. Nanosilicate-hydrogel microspheres formed by aqueous two-phase separation for sustained release of small molecules. *Front. Biomater. Sci.* **2023**, *2*, 1157554.
- (12) Byun, C. K. Partitional Behavior of Janus Dumbbell Microparticles in a Polyethylene Glycol (PEG)-Dextran (DEX) Aqueous Two-Phase System (ATPS). *Coatings* **2022**, *12* (3), 415.
- (13) Mohsen Dehnavi, S.; Pazuki, G.; Vossoughi, M. PEGylated silica-enzyme nanoconjugates: a new frontier in large scale separation of α -amylase. *Sci. Rep.* **2016**, *5*, 18221.
- (14) Nouri, M.; Shahriari, S.; Pazuki, G. Increase of vanillin partitioning using aqueous two phase system with promising nanoparticles. *Sci. Rep.* **2019**, *9*, 19665.
- (15) Kostiv, U.; Farka, Z.; Mickert, M. J.; Gorris, H. H.; Velychkiivska, N.; Pop-Georgievski, O.; Pastucha, M.; Odstrčilíková, E.; Skládal, P.; Horák, D. Versatile Bioconjugation Strategies of PEG-Modified Upconversion Nanoparticles for Bioanalytical Applications. *Biomacromolecules* **2020**, *21* (11), 4502–4513.
- (16) Höldrich, M.; Sievers-Engler, A.; Lämmerhofer, M. Gold nanoparticle-conjugated pepsin for efficient solution-like heterogeneous biocatalysis in analytical sample preparation protocols. *Anal. Bioanal. Chem.* **2016**, *408*, 5415–5427.
- (17) Retout, M.; Blond, P.; Jabin, I.; Bruylants, G. Ultrastable PEGylated Calixarene-Coated Gold Nanoparticles with a Tunable Bioconjugation Density for Biosensing Applications. *Bioconjugate Chem.* **2021**, *32* (2), 290–300.
- (18) Couto, C.; Vitorino, R.; Daniel-da-Silva, A. L. Gold nanoparticles and bioconjugation: a pathway for proteomic applications. *Crit. Rev. Biotechnol.* **2017**, *37* (2), 238–250.
- (19) Bansal, S. A.; Kumar, V.; Karimi, J.; Singh, A. P.; Kumar, S. Role of gold nanoparticles in advanced biomedical applications. *Nanoscale Adv.* **2020**, *2*, 3764–3787.
- (20) Long, M. S.; Keating, C. D. Nanoparticle Conjugation Increases Protein Partitioning in Aqueous Two-Phase Systems. *Anal. Chem.* **2006**, *78* (2), 379–386.
- (21) Duan, X.; Liu, B. A facile method for purifying DNA-modified small particles and soft materials using aqueous two-phase systems. *Chem. Commun.* **2023**, *59*, 9130–9133.
- (22) Myers, R. H.; Montgomery, D. C.; Anderson-Cook, C. M. *Response Surface Methodology: Process and Product Optimization Using Designed Experiments*, 4th ed.; John Wiley & Sons, Inc.: NJ, 2016.
- (23) Chen, F.; Huang, G.; Huang, H. Preparation and application of dextran and its derivatives as carriers. *Int. J. Biol. Macromol.* **2020**, *145*, 827–834.
- (24) Deb, P. K.; Al-Attraqchi, O. H. A.; Stanslas, J.; Al-Aboudi, A.; Al-Attraqchi, N.; Tekade, R. K. Advances in Pharmaceutical Product Development and Research, Biotechnology-Based Pharmaceutical Products. In *Biomaterials and Bionanotechnology*; Tekade, R. K., Ed.; Academic Press: London, 2019; pp 153–189.
- (25) Fakhari, M. A.; Rahimpour, F.; Taran, M. Response surface methodology optimization of partitioning of xylanase from *Aspergillus Niger* by metal affinity polymer-salt aqueous two-phase systems. *J. Chromatogr. B* **2017**, *1063*, 1–10.
- (26) Rahimpour, F.; Mamo, G.; Feyzi, F.; Maghsoudi, S.; Hatti-Kaul, R. Optimizing refolding and recovery of active recombinant Bacillus halodurans xylanase in polymer-salt aqueous two-phase system using surface response analysis. *J. Chromatogr. A* **2007**, *1141* (1), 32–40.
- (27) Rahimpour, F.; Feyzi, F.; Maghsoudi, S.; Hatti-Kaul, R. Purification of plasmid DNA with polymer-salt aqueous two-phase system: Optimization using response surface methodology. *Biotechnol. Bioeng.* **2006**, *95* (4), 627–637.
- (28) Lanjekar, K. J.; Rathod, V. K. Response surface methodology for optimization of glycyrrhizic acid extraction from *Glycyrrhiza glabra* in the aqueous two-phase system. *Indian Chem. Eng.* **2023**, *65* (1), 38–50.

- (29) Grabar, K. C.; Freeman, R. G.; Hommer, M. B.; Natan, M. J. Preparation and Characterization of Au Colloid Monolayers. *Anal. Chem.* **1995**, *67* (4), 735–743.
- (30) Yahya, N. A.; Wahab, R. A.; Attan, N.; Hashim, S. E.; Abdul Hamid, M.; Mohamed Noor, N.; Abdul Rahman, A. Optimization of oil-in-water nanoemulsion system of Ananas comosus peels extract by D-optimal mixture design and its physicochemical properties. *J. Dispersion Sci. Technol.* **2022**, *43* (2), 302–315.
- (31) Jiang, B.; Wang, L.; Zhu, M.; Wu, S.; Wang, X.; Li, D.; Liu, C.; Feng, Z.; Tian, B. Separation, structural characteristics and biological activity of lactic acid bacteria exopolysaccharides separated by aqueous two-phase system. *Lebensm. Wiss. Technol.* **2021**, *147*, 111617.
- (32) Liu, J.; Bai, J.; Shao, C.; Yao, S.; Xu, R.; Duan, S.; Wang, L.; Xu, Y.; Yang, Y. Optimization of ultrasound-assisted aqueous two-phase extraction of polysaccharides from seabuckthorn fruits using response methodology, physicochemical characterization and bioactivities. *J. Sci. Food Agric.* **2023**, *103* (6), 3168–3183.
- (33) Fagúndez, P.; Botasini, S.; Tosar, J. P.; Mendez, E. Systematic process evaluation of the conjugation of proteins to gold nanoparticles. *Heliyon* **2021**, *7*, No. e07392.
- (34) Golkar, N.; Sarikhani, Z.; Aghaei, R.; Heidari, R.; Amini, A.; Gholami, A. An oral nanoformulation of insulin: Development and characterization of human insulin loaded graphene oxide-sodium alginate-gold nanocomposite in an animal model. *J. Drug Delivery Sci. Technol.* **2023**, *82*, 104309.
- (35) Delbeck, S.; Heise, H. M. FT-IR versus EC-QCL spectroscopy for biopharmaceutical quality assessment with focus on insulin—total protein assay and secondary structure analysis using attenuated total reflection. *Anal. Bioanal. Chem.* **2020**, *412*, 4647–4658.
- (36) Ebrahimi, A.; Pazuki, G.; Mozaffarian, M.; Ahsaie, F. G.; Abedini, H. Separation and Purification of C-Phycocyanin from *Spirulina platensis* Using Aqueous Two-Phase Systems Based on Triblock Thermosensitive Copolymers. *Food Bioprocess Technol.* **2023**, *16*, 2582–2597.
- (37) Bedade, D.; Pawar, S. Downstream processing of biotechnology products. In *Basic Biotechniques for Bioprocess and Bioentrepreneurship*; Bhatt, A. K., Bhatia, R. K., Bhalla, T. C., Eds.; Academic Press, 2023; pp 377–390.
- (38) Chen, G. Q.; Qu, Y.; Gras, S. L.; Kentish, S. E. Separation Technologies for Whey Protein Fractionation. *Food Eng. Rev.* **2023**, *15*, 438–465.
- (39) Huang, J.; Laaser, J. E. Charge Density and Hydrophobicity-Dominated Regimes in the Phase Behavior of Complex Coacervates. *ACS Macro Lett.* **2021**, *10* (8), 1029–1034.
- (40) Santos, J. J.; Leal, J.; Dias, L. A. P.; Toma, S. H.; Corio, P.; Genezini, F. A.; Katti, K. V.; Araki, K.; Lúgão, A. B. Bovine Serum Albumin Conjugated Gold-198 Nanoparticles as Model To Evaluate Damage Caused by Ionizing Radiation to Biomolecules. *ACS Appl. Polym. Mater.* **2018**, *1* (9), 5062–5070.
- (41) Wang, C.; Zhang, Z.; Wang, Q.; Wang, J.; Shang, L. Aqueous two-phase emulsions toward biologically relevant applications. *Trends Chem.* **2023**, *5* (1), 61–75.
- (42) Singla, M.; Sit, N. Isolation of papain from ripe papaya peel using aqueous two-phase extraction. *J. Food Meas. Char.* **2023**, *17*, 1685–1692.
- (43) Khan, I.; Saeed, K.; Khan, I. Nanoparticles: Properties, applications and toxicities. *Arab. J. Chem.* **2019**, *12* (7), 908–931.
- (44) Iriarte-Mesa, C.; López, Y. C.; Matos-Peralta, Y.; de la Vega-Hernández, K.; Antuch, M. Gold, Silver and Iron Oxide Nanoparticles: Synthesis and Bionanoconjugation Strategies Aimed at Electrochemical Applications. *Top. Curr. Chem.* **2020**, *378*, 12.